A localization algorithm for railway vehicles based on sensor fusion between tachometers and inertial measurement units

A localization algorithm for railway vehicles based on sensor fusion between tachometers and inertial measurement units

M Malvezzi, G Vettori, B Allotta, L Pugi, A Ridolfi and A Rindi

Proceedings of the Institution of Mechanical Engineers, Part F: Journal of Rail and Rapid Transit 2014 228: 431 originally published online 9 April 2013
DOI: 10.1177/0954409713481769

Original Article

Institution of MECHANICAL ENGINEERS
Journal of RAIL AND RAPID TRANSIT

Proc IMechE Part F:
J Rail and Rapid Transit
2014, Vol. 228(4) 431–448

DOI: 10.1177/0954409713481769
pif.sagepub.com
SAGE

A localization algorithm for railway vehicles based on sensor fusion between tachometers and inertial measurement units

M Malvezzi[1], G Vettori[2], B Allotta[2], L Pugi[2], A Ridolfi[2] and A Rindi[2]

Abstract

The availability of a reliable speed and travelled distance estimation is relevant for the efficiency and safety of automatic train protection and control systems. This paper investigates the main features of an innovative localization algorithm that integrates tachometers and inertial measurement units. Nowadays, the estimation is performed by an odometry algorithm that relies on wheel angular speed sensors. The objective is to increase the accuracy of the odometric estimation, especially in critical adhesion conditions, through sensor fusion techniques based on Kalman filter theory. The Italian company ECM S.p.A. has supported the project, providing a custom inertial measurement unit based on micro electro-mechanical system sensors for the on-track testing of the algorithm. The preliminary results show a significant improvement of the position and speed estimation performances compared to those obtained with SCMT (Italian acronym for 'Sistema Controllo Marcia Treno') algorithms, currently in use on the Italian railway network. A wide set of simulated test results, showing the improvement of the estimation process, is presented and discussed. An accurate train navigation that scarcely relies on information from the infrastructure will open a road map for the development of a more and more effective and efficient exploitation of the railway infrastructure.

Keywords

Automatic train protection and control safety systems, odometry railway applications, localization algorithms, micro electro-mechanical system inertial sensors, Kalman filter, sensor fusion

Date received: 17 October 2012; accepted: 14 February 2013

Introduction

The importance of monitoring and control systems is continuously growing in the modern railway network. Automatic train protection and control (ATP-ATC) systems are fundamental to increase the infrastructure capacity, by maintaining a proper level of operation safety.

Odometry is a relevant on-board module that estimates instantaneously the speed and the travelled distance of a railway vehicle by dead reckoning; the availability of a reliable speed and travelled distance estimation is the base of a safe and efficient ATP-ATC system, since an error on the train position may lead to a potentially dangerous overestimation of the distance available for braking.

The European Rail Traffic Management System (ERTMS), a project developed by the European Union to improve the interoperability between different countries, in particular as regards the train control and command systems, fixes some standard values for the odometric performance, in terms of speed and travelled distance reliability.[1–4] The reliability of the odometric estimation has to be taken into account in the definition of allowed speed profiles.[5–7]

Typically, in railway applications, the dead reckoning relies on wheel angular speed sensors, but other types of sensors can be used: radar Doppler sensors, accelerometers, gyroscopes, etc.[8,9] A novel method for the estimation of the train is the use of traction motor and current.[10] Generally, one isolated sensor can partially provide accurate data since its reliability ranges are often limited; furthermore, the environmental

[1]Department of Information Engineering, University of Siena, Siena, Italy
[2]Department of Industrial Engineering, University of Florence, Florence, Italy

Corresponding author:
Gregorio Vettori, Department of Industrial Engineering, University of Florence, Via Santa Marta 3, Florence 50139, Italy.
Email: gregorio.vettori@unifi.it

conditions may vary during the train operation, in an unpredictable and unquantifiable way.

The reliability of dead reckoning is then related to the working conditions in which the sensors operate.[11,12] For instance, wheel angular speed sensors located on two independent wheels give a reliable and accurate estimation of the train speed, but only when good adhesion conditions between the wheel and rail occur.[13,14] In the presence of wheel sliding (when the train is accelerating or braking), the estimation error may become very high.

Sensor fusion techniques based on Kalman filter theory have the potential to compensate the drawbacks of a single sensor, combining information from independent sources, each characterized by limited accuracy and reliability, in order to extract better information. Furthermore, the use of different types of sensors, whose information is properly weighted according to specific operative conditions, may significantly increase the algorithm reliability[12] and reduce system vulnerability to failures of single components.

Georeferentation of the track lines could be a possibility for accurate estimation of the position. In this way, odometry could take advantage of global positioning systems (GPSs) to detect each point on the track as longitude, latitude and height, and match it to the length of the line up to that point. However, in railway applications, the lack of georeferentation and the outages of signals, e.g. in tunnels, discourage the use of GPSs.

The analysis of the methods and results described in Malvezzi et al.[8] suggests that an accurate measure of longitudinal acceleration could significantly improve the recognition of degraded adhesion conditions, and could be used to estimate the train speed and position when wheel speed sensors fail due to slip and slide phenomena.

A mono-axial accelerometer was used to measure the longitudinal acceleration, but the measure was affected by systematic errors, due to the sensor sensitivity to car body angular displacement, mainly due to the track gradient. In Malvezzi et al.,[8] the dependency of the accelerometer measure on the train pitch and angular position error was analysed, and an odometry algorithm was developed in order to be not very sensitive to such types of errors.

An estimation of the train longitudinal acceleration less sensitive to sensor angular displacements may be obtained by combining accelerometers and gyroscopes.[11] Moreover, the rapid technological development of low-cost micro electro-mechanical systems (MEMSs) sensors made the integration of an inertial measurement unit (IMU) into the odometric estimation very interesting. Both the definition of an innovative localization algorithm and the design of a low-cost custom IMU meet the need of the Italian company ECM S.p.A. to develop a competitive industrial product able to enhance the reliability of the odometric estimation.

The aim of the work is to provide an innovative solution able to increase the accuracy of the odometric estimation, compared to the commonly adopted solutions, which have often lack of reliability: SCMT (Italian acronym for 'Sistema Controllo Marcia Treno') algorithms, for example, are forced to overestimate the speed for safety scopes, so the emergency braking occurs more than required. The objective to keep the accuracy high, i.e. limited estimation error, allows an increase of the performance of the ATP system and achieves a more reliable system in terms of comfort and consumption.

In this paper, the design of a pose estimation algorithm that integrates odometers and an inertial navigation system (INS) based on an inertial measurement unit (IMU) is described. The developed algorithm has been validated with a set of simulated scenarios realized with a three-dimensional (3D) multibody dynamic model of a railway vehicle able to reproduce most of the conditions that may affect the reliability of the sensors.[15]

The paper is organized as follows. In the next section, the different kinds of sensors that are used for the proposed localization algorithm are analysed: wheel angular speed sensors and inertial sensors (triaxial accelerometers and gyroscopes). Then, the sensor fusion between tachometers and the IMU is shown, and the testing procedure and the European train control systems (ETCS) requirements[1–4] are explained. Finally, a comparison of the proposed localization strategy with the SCMT solution, in terms of estimation accuracy, is presented and discussed.

Sensors for odometry

Different types of sensors can be used in the odometry subsystem; the main features of the sensors used to perform the preliminary tests are briefly described in this section. The sensors considered and analysed by means of experimental activities and numerical simulations are wheel angular speed sensors and inertial sensors (triaxial accelerometers and gyroscopes).

The analysis of other types of sensors, e.g. radar Doppler speed sensors and mono-axial accelerometers, is discussed in Malvezzi et al.,[8] while a discussion on sensors for railway applications is presented in Mirabadi et al.[11]

Wheel angular speed sensors (tachometers)

Wheel angular speed sensors are widely diffused in railway applications due to their robustness and reliability: they are used, e.g. by the wheel slide protection (WSP) and anti-skid systems. Through this type

of sensors, when pure rolling conditions occur, the train speed can be simply calculated as

$$v = R\omega \tag{1}$$

where v is the longitudinal train speed, ω is the wheel angular speed and R is the wheel radius.

It is worth noting that the wheel radius information sometimes may not be reliable, since railway wheels are subject to wear and periodical mechanical returnings. The weak point is the low reliability under degraded adhesion conditions, which is rather common in railway practice. If the wheel is not sliding, this sensor provides a good and reliable estimation of the train speed, but, when the wheel–rail adhesion conditions are degraded, and the train is accelerating or braking, pure rolling conditions between the wheel and the rail do not hold any more and macroscopic slidings arise. If the train is accelerating, the wheel peripheral speed tends to overcome the train speed, while during the braking phase, the wheel peripheral speed is lower than the train one. The dynamics of the wheels in sliding mode significantly depends on the mechanical feature of the vehicle (masses and inertia, geometric properties, suspension characteristics, etc.) and on the interactions between the different on-board subsystems, in particular, the braking system and the WSP, the traction system and the anti-skid. The sensor output is a signal proportional to the pulse counter c, in the generic time sample i. The wheel angular speed ω_i can be evaluated by finite derivatives as

$$\omega_i = \frac{2\pi}{N}\frac{(c_i - c_{i-1})}{\Delta T} \tag{2}$$

where c_i is the current sample, c_{i-1} is the preceding sample, N is the number of impulses per revolution, ΔT is the sampling time. SCMT, the Italian ATP system, supports an odometry algorithm[13,14] based on the measures from two angular speed sensors. The adhesion conditions are estimated by means of two criteria:

- the so-called *tachometric criterion* states that two wheels (or at least one of them) are sliding or skidding if the absolute value of the difference between their wheel peripheral speeds (v_1, v_2) overcomes a fixed threshold (Δ_v)

$$|v_1 - v_2| > \Delta_v \tag{3}$$

- the *accelerometric criterion* compares the wheel peripheral accelerations: a wheel is sliding if the absolute value of its acceleration (a_1, a_2) overcomes a fixed threshold (Δ_a)

$$|a_1| > \Delta_a \quad |a_2| > \Delta_a \tag{4}$$

The detection of the condition of the adhesion shows some weak points: in fact, if both wheels slide, the possibility that the 'tachometric criterion' fails is high, as actually happens in practical applications. In this case, the 'accelerometric criterion' should be able to recognize the sliding phase. In the worst-case scenario of sliding of all the wheels and with low acceleration, both the criteria may fail. The fake detection of the adhesion condition happens frequently on the railway network, so the SCMT algorithm is often affected by non-negligible errors. If the estimated adhesion conditions are judged as 'good', according to the previously mentioned criteria, the train speed can be evaluated directly from the peripheral speeds of the wheels. When the wheels are sliding and the train is accelerating (or braking), the speed can be evaluated as the minimum (maximum) between the speeds of the two wheels, and a speed estimate obtained by integrating a constant acceleration (deceleration) value, previously established, according to the dynamical performances of the train.

IMUs

An IMU is an electronic device composed of a triaxial accelerometer and a triaxial gyroscope. It can measure triaxial body frame acceleration

$$\vec{f}^b = \left[f_x^b\ f_y^b\ f_z^b\right]^{\mathrm{T}} \tag{5}$$

and triaxial body frame angular rate

$$\vec{w}_{ib}^b = \left[w_x^b\ w_y^b\ w_z^b\right]^{\mathrm{T}} \tag{6}$$

The accelerometer provides an output proportional to the non-gravitational force per unit mass (f) to which the sensor is subjected along its sensitive axis (an acceleration dimensionally). In order to calculate the acceleration due to the movement (a), the following operation must be performed

$$a = f + g \tag{7}$$

Gyroscopes measure angular rates corresponding to rotations of the platform where the IMU is mounted with respect to an *i-frame* inertial frame, with non-rotating axes with respect to the fixed stars, i.e. the invoked inertial reference frame.

Classical IMUs are very expensive and very accurate, but modern accelerometers and gyroscopes are often small MEMSs with low cost and quite high noise. The primary sources of accelerometer and gyroscope errors (e_a and e_g, respectively) include sensor noise, scale-factor errors, cross-axis coupling factors and bias.[11] Thus, the inertial sensor measurement equations for both the accelerometer and the gyroscope are

$$\bar{f} = f + e_a = f + b_a + S_a f + m_a f + \eta_a$$
$$\bar{w} = w + e_g = w + b_g + S_g w + m_g w + \eta_g$$

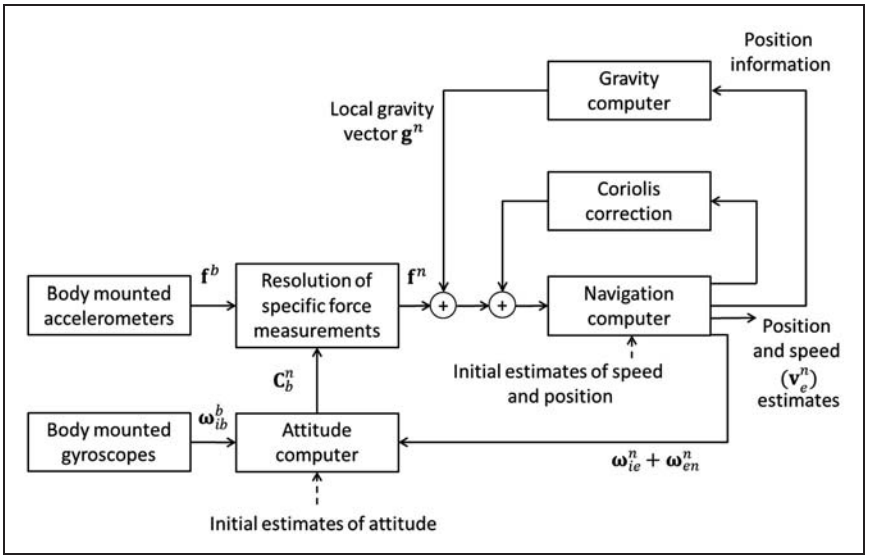

Figure 1. INS algorithm.

where $\tilde{\cdot}$ denotes the measured value by the sensor and the subscripts a and g mean the accelerometer-specific errors the gyroscope-specific errors respectively. The symbols in the above equations mean: f is the specific force as previously defined, w is the angular rate, b is the sensor bias, S is the scale-factor error, m is the assembly error and η is the sensor random noise. The bias is generally composed of two parts, a deterministic bias offset and a bias drift. The outputs of the IMU can be processed to determine the position, velocity and attitude of a vehicle through algorithms called the INS. The classical architecture of an INS algorithm is shown in Figure 1.[16]

The following reference frames are defined: *e-frame* (Earth frame) with axes fixed with respect to the Earth, *n-frame* (navigation frame) with axes fixed with respect to the east, north and up directions and the *b-frame* (body frame) with axes aligned with the vehicle. The rotation matrix C_b^n expresses the relationship between the navigation and body frame, and is used to transform the acceleration measurements from the *b-frame* to the *n-frame*, thus

$$a^n = C_b^n f^b + g^n \tag{8}$$

where f^b is the quantity defined in equation (5) and g^n is the gravity vector equal to $[0\ 0\ -9.81]^{\mathrm{T}}$.

It is worth noting that, for the scope of this work, the contributions of ω_{ie}^n (Earth's rate with respect to the *i-frame*) and ω_{en}^n (turn rate of the *n-frame* with respect to the Earth) are considered negligible, since they are much less than the signal from the movement, thus

$$\omega_{ib}^b = \omega_{nb}^b \tag{9}$$

The attitude computation is usually quaternion based

$$q(k+1) = q(k) + \frac{1}{2}\Omega_k q(k) dt \tag{10}$$

where Ω_k is the 4×4 skew symmetric matrix based on angular rates $(\omega_x^b\ \omega_y^b\ \omega_z^b)$. The quaternion $q = [\eta\ \epsilon_x\ \epsilon_y\ \epsilon_z]$, unlike the Euler angles, avoids the occurrence of singularities and permits calculation of C_b^n

$$C_b^n = \begin{bmatrix} 2(\eta^2+\epsilon_x^2)-1 & 2(\epsilon_x\epsilon_y-\eta\epsilon_z) & 2(\epsilon_x\epsilon_z+\eta\epsilon_y) \\ 2(\epsilon_x\epsilon_y+\eta\epsilon_z) & 2(\eta^2+\epsilon_y^2)-1 & 2(\epsilon_y\epsilon_z-\eta\epsilon_x) \\ 2(\epsilon_x\epsilon_z-\eta\epsilon_y) & 2(\epsilon_y\epsilon_z+\eta\epsilon_x) & 2(\eta^2+\epsilon_z^2)-1 \end{bmatrix}$$

It is then possible to estimate the velocity of the vehicle through an integration of the transformed acceleration and the position in a fixed reference through a double integration.

This algorithm blindly processes the raw inertial data affected by errors. The performed time integration introduces drift errors in the estimate. The orientation error ($\delta\Phi$), from the integration of the angular rates, causes an incorrect projection of the acceleration signals onto the global axes, i.e. a tilt error ($\delta\theta = e_g t$) will cause a component of the acceleration due to gravity with magnitude $g\sin(\delta\theta)$ to be projected onto the horizontal axes. This error propagates on the velocity and position according to

$$\begin{aligned}
\delta v &= \hat{v} - v = \int \bar{a}\,\mathrm{d}t - v \\
&= \int a\,\mathrm{d}t + \int e_a\,\mathrm{d}t + \int g e_g t\,\mathrm{d}t - v \\
&= v + e_a t + \frac{1}{2} e_g g t^2 - v = e_a t + \frac{1}{2} e_g g t^2 \\
\delta p &= \hat{p} - p = \int \hat{v}\,\mathrm{d}t - p = \int e_a t\,\mathrm{d}t + \int \frac{1}{2} e_g g t^2\,\mathrm{d}t - p \\
&= p + \frac{1}{2} e_a t^2 + \frac{1}{6} e_g g t^3 - p = \frac{1}{2} e_a t^2 + \frac{1}{6} e_g g t^3
\end{aligned}$$

Deterministic compensation is not sufficient to erase the error due to random white noise. Stochastic filters such as extended Kalman filter (EKF) can improve the estimation performances of

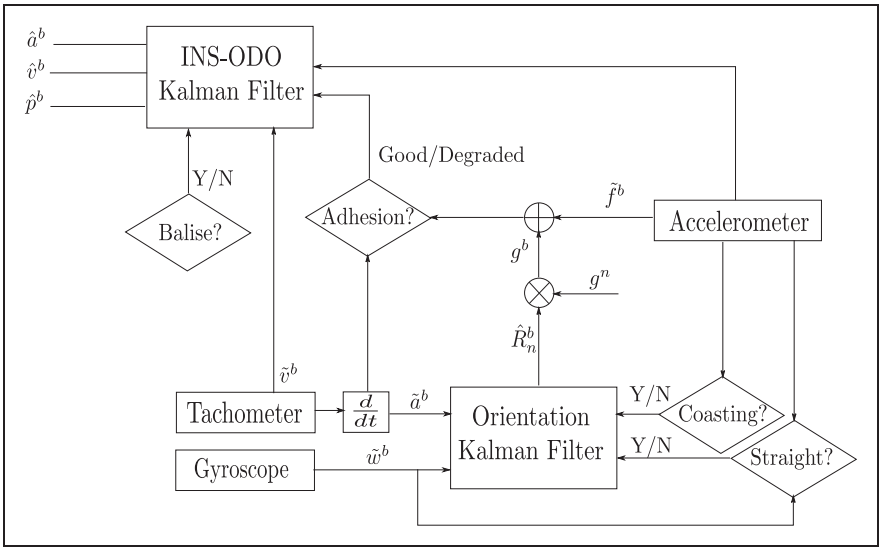

Figure 2. Block diagram of the localization algorithm.

INS algorithms. EKF equations for inertial navigation are described in Barshan and Durrant-Whyte[17] and consist of a linear state transition model and a non-linear observation model.

Stochastic filters reduce the integration error, but cannot provide the high accuracy level required for this application. In these cases, higher quality information can be achieved using multiple sensors and integrating them.

There are different methods of data fusion that have been developed for different types of sensors and applications. Kalman filtering has more potential for integration of navigation sensors, where sensor data are used as observations.

Sensor fusion between odometers and INSs

In this section, the architecture of the innovative localization algorithm is presented. As stated previously, the INS cannot provide the high accuracy required for velocity and position estimates.

According to the sensor fusion techniques that allow the integration of the measures from different sources, attempting to choose, in each condition, the sensor that has the maximum reliability, and to identify and compensate the sensor measurement error, the INS estimation is *fused* with the tachometer measurement, in order to optimize the odometric estimation accuracy.

Compared to previously introduced odometry algorithms,[8,13] the proposed algorithm can take advantage of sensor fusion techniques, through the integration of the INS with a wheel angular speed sensor and the reset of the position estimation when a balise occurs along the track.

Some preliminary numerical experiments and considerations have led to the idea of separating the 3D attitude estimation and the one-dimensional (1D) speed/travelled distance estimation. In this way, the comparison between the speed estimated by the integration of the accelerometer and the speed measured by the tachometer, and also the reset of the estimate of the travelled distance corresponding to a balise, are simply and directly available. Moreover, ETCS requirements,[1–4] which are used to test the performances of odometry algorithms, are based on the longitudinal speed error and the travelled distance error.

The proposed algorithm is summarized by the block diagram in Figure 2, where $\hat{R}_n^b$ represents the rotation matrix from the *n-frame* (defined as the initial body frame of the vehicle) to the *b-frame* and $\vec{g}$ is the gravitational vector.

As can be seen in this diagram, two Kalman filters are implemented:

- the *orientation Kalman filter* estimates the Euler angles (roll, pitch, yaw) from the *b-frame* to the *n-frame*, fusing the information of the angular rate from the gyroscope with the wheel peripheral acceleration, derived from the tachometer;
- the *INS-ODOmetry Kalman filter* estimates speed and travelled distance, fusing the gravity compensated body longitudinal acceleration with the wheel peripheral speed.[13]

As shown in Figure 2, the algorithm provides four *diamond* boxes, related to relevant working conditions (coasting, straight, adhesion, balise). Their meaning is explained in the subsections below.

Orientation Kalman filters

The state equation of the orientation Kalman filter in block matrix form is

$$\vec{x}_{Gi}(k+1) = F_{Gi}\vec{x}_{Gi}(k) \tag{11}$$

where $i = x, y, z$ and

$$\vec{x}_{Gx} = \left[\psi\ \dot{\psi}\right]^{\mathrm{T}}$$

$$\vec{x}_{Gy} = \left[\theta\ \dot{\theta}\right]^{\mathrm{T}}$$

$$\vec{x}_{Gz} = \left[\phi\ \dot{\phi}\right]^{\mathrm{T}}$$

where ψ, θ and ϕ are, respectively, the roll, pitch and yaw angles, $\dot{\psi}$, $\dot{\theta}$ and $\dot{\phi}$ are their derivatives with respect to time, and the matrix F_G is defined as

$$F_{Gi} = \begin{bmatrix} 1 & T_s \\ 0 & 1 \end{bmatrix}$$

with $i = x, y, z$ and T_s is the sampling time (equal to 0.1 s, in accordance with the sampling time of classical odometry algorithms).

The process noise covariance matrix Q_G is assumed as

$$Q_G = \mathrm{diag}(Q_{Gx}, Q_{Gy}, Q_{Gz}),$$

$$Q_{Gi} = \begin{bmatrix} \frac{T_s^3}{3}\sigma_i^2 & \frac{T_s^2}{2}\sigma_i^2 \\ \frac{T_s^2}{2}\sigma_i^2 & T_s\sigma_i^2 \end{bmatrix} \tag{12}$$

with $i = x, y, z$; in this equation, σ_i values represent the experimentally determined standard deviations of the components of the state vector.

The observation array is

$$\vec{z}_G = \begin{bmatrix} \bar{\omega}_x^b \\ \bar{\omega}_y^b \\ \bar{\omega}_z^b \\ \bar{a}_x^b \\ 0 \end{bmatrix} \tag{13}$$

The first three components are the *b-frame* angular rates measured by the gyroscope; the fourth is the longitudinal component of the *b-frame* acceleration obtained by the finite derivatives (Euler backward method) of two subsequent tachometer measures

$$\bar{a}_x^b(i) = \frac{\bar{v}_x^b(i) - \bar{v}_x^b(i-1)}{T_s} \tag{14}$$

where i is the time sample.

The last component is the zero value for the reset of the roll angle that can occur in the particular condition of straight track.

The H_G matrix, which correlates observations with the state is

$$H_G = \begin{bmatrix} 0 & 1 & 0 & 0 & 0 & -s\theta \\ 0 & 0 & 0 & c\psi & 0 & c\theta s\psi \\ 0 & 0 & 0 & -s\psi & 0 & c\theta c\psi \\ 0 & 0 & g_z & 0 & 0 & 0 \\ 1 & 0 & 0 & 0 & 0 & 0 \end{bmatrix}$$

where $s\theta = \sin(\theta)$ and $c\theta = \cos(\theta)$ and $g_z = -9.81\ \mathrm{m/s^2}$.

Since pitch angles are small, the following approximation can be assumed

$$a_x = g_z \sin(\theta) \approx g_z\theta \tag{15}$$

The sensor noise covariance matrix R_G is assumed as

$$R_G = \mathrm{diag}(\sigma_{\omega_x}^2, \sigma_{\omega_y}^2, \sigma_{\omega_z}^2, \sigma_{a_b}^2, \sigma_0^2) \tag{16}$$

where the elements in the diagonal matrix are the standard deviations of the sensor measures.

The R_G matrix is adaptive with respect to the conditions *coasting* and *straight* represented in the diamond boxes in Figure 2.

Coasting is a phase where neither traction and braking occur. Since a movement caused only by the line gradient is compensated by the gravity term (equation (7)), the coasting phase is related to the fact that the longitudinal component of the accelerometer is close to 'zero'. In this case, the wheel peripheral acceleration (equation (14)) is substantially equal to the longitudinal acceleration, since in the coasting phases, the phenomena of degraded adhesion do not have any effect. In this way, it is possible to retrieve a reliable estimate of the line gradient, through the inversion of equation (15) (taken into account in the H_G matrix), from a source decoupled from the gyroscopes

$$\begin{cases} \sigma_{\omega_y}^2 \gg \sigma_{a_b}^2, & \text{if } \left|\bar{f}_x^b\right| < \eta_{f_x} \\ \sigma_{\omega_y}^2 \ll \sigma_{a_b}^2, & \text{otherwise} \end{cases} \tag{17}$$

Equation (17) explains how the coasting phase is handled by the orientation Kalman filter. When 'zero' longitudinal accelerations occur, sensor noise covariance values ($\sigma_{\omega_y}^2$ and $\sigma_{a_b}^2$) are set to enable the contribution of the tachometer and disable the component y of the gyroscope.

Instead, the complementary case occurs when the longitudinal component of the accelerometer is far from zero (traction and braking phases).

The straight condition states the reset of the roll angle: in fact, neglecting roll variations due to the

suspension dynamics, relevant values of this angle occur when the track is curvilinear, in the presence of *cant* angles.

The requirement of 'zero' lateral acceleration is not sufficient to state the absence of curved track: in fact, the compensation of the total lateral acceleration can subsist when the centrifugal acceleration, due to the train motion in curve, is compensated by the 'gravity lateral acceleration', due to the presence of *cant* in the curves of a railway track. Therefore, it is necessary to include conditions on the gyroscopes, that is 'zero' angular rates over the x and z axes

$$\begin{cases} \sigma^2_{\omega_x} \gg \sigma^2_0, & \text{if}\left(\left|\bar{f}^b_y\right| < \eta_{f_y} \;\&\; \left|\bar{\omega}^b_x\right| < \eta_{\omega_x} \;\&\; \left|\bar{\omega}^b_z\right| < \eta_{\omega_z}\right) \\ \sigma^2_{\omega_x} \ll \sigma^2_0, & \text{otherwise} \end{cases} \tag{18}$$

Condition (18) allows 'turning on' the contribution of the roll reset when the three requirements explained ('zero' lateral acceleration, 'zero' x and z angular rates) occur at the same time.

The thresholds η_{f_x}, η_{f_y}, η_{ω_x}, η_{ω_z} have been experimentally tuned (see the subsection on simulated sensor masks).

INS/ODO Kalman filters

The state equations of the INS/ODO Kalman filter, expressed in block matrix form, are

$$\begin{bmatrix} p^b_x(k+1) \\ v^b_x(k+1) \\ a^b_x(k+1) \end{bmatrix} = \begin{bmatrix} 1 & T_s & \frac{1}{2}T_s^2 \\ 0 & 1 & T_s \\ 0 & 0 & 1 \end{bmatrix} \begin{bmatrix} p^b_x(k) \\ v^b_x(k) \\ a^b_x(k) \end{bmatrix}$$

where p^b_x is the distance travelled by the train, v^b_x is the train speed and a^b_x is the *b-frame* acceleration.

The process noise covariance matrix Q_A is assumed as

$$Q_A = \begin{bmatrix} \frac{T_s^5}{20}\sigma_a^2 & \frac{T_s^4}{8}\sigma_a^2 & \frac{T_s^3}{6}\sigma_a^2 \\ \frac{T_s^4}{8}\sigma_a^2 & \frac{T_s^3}{3}\sigma_a^2 & \frac{T_s^2}{2}\sigma_a^2 \\ \frac{T_s^3}{6}\sigma_a^2 & \frac{T_s^2}{2}\sigma_a^2 & T_s\sigma_a^2 \end{bmatrix}$$

where σ_a represents the experimentally determined standard deviation of the components of the state vector.

The observation array is

$$\vec{z}_A = \begin{bmatrix} f^b_x + R^b_n g^n \\ v^b_x \\ 0 \end{bmatrix} \tag{19}$$

The first component is the compensated longitudinal gravity acceleration, the second is the speed of the train measured by the tachometer and the third is the zero point of the position reset sent by the balise, which is supposed to occur each 1000 m.

The H_a matrix, which correlates the observations with the state, is

$$H_a = I_{3x3} \tag{20}$$

The sensor noise covariance matrix R_A is assumed as

$$R_A = \text{diag}(\sigma^2_{a_x}, \sigma^2_{v_x}, \sigma^2_{p_x}) \tag{21}$$

where the elements in the diagonal are the standard deviation values of the sensor measures.

The R_A matrix is adaptive with respect to the conditions *adhesion* and *balise* represented in the diamond boxes in Figure 2.

The adhesion condition is determined through the condition reported in equation (22). The master criterion is the 'accelerometric criterion': if the difference between the wheel peripheral acceleration (a^b_x) and the gravity compensated body longitudinal acceleration ($f^b_x - \hat{R}^b_n g^n$) is less than a threshold (η_{ad}), the adhesion is considered good. In order to avoid that 'fake' good adhesion conditions are considered, a slave 'tachometric criterion' has been implemented: it allows the speed to be reset only if the difference between the actual estimated speed ($\hat{v}^b$) and the wheel peripheral speed (v^b_x) is lower than a threshold (η_v). It is worth noting that, with respect to the classical SCMT solutions, only one tachometer is sufficient for the detection of the wheel–rail adhesion condition

$$\begin{cases} \sigma^2_{a_x} \gg \sigma^2_{v_x}, & \text{if}\left(\left|f^b_x - \hat{R}^b_n g^n - a^b_x\right| < \eta_{ad} \;\&\; \left|\hat{v}^b - v^b_x\right| < \eta_v\right) \\ \sigma^2_{a_x} \ll \sigma^2_{v_x}, & \text{otherwise} \end{cases} \tag{22}$$

Equation (22) states that, when good adhesion between the wheel and the rail occurs, the measurement update of the Kalman filter can rely on the contribution of the speed measures provided by the tachometer. Moreover, although degraded adhesion conditions occur, the longitudinal acceleration signal provides an estimate of speed and travelled distance.

The thresholds η_{ad} and η_v have been experimentally tuned in the testing phase.

The balise condition (23) allows the travelled distance estimate to be reset, through a recognition of the occurrence of a balise. During the operative conditions a logic signal reveals the presence of a balise. In a simulated scenario, it was hypothesized that a balise occurred every 1000 m, assuming a 5 m bidirectional error (expressed by η_{ba}) on its positioning along

the track. This value of uncertainty is obtained considering empirical knowledge about the tolerances linked to the balise positioning along the line

$$\begin{cases} \sigma_{a_x}^2 \gg \sigma_{r_x}^2, & \text{if } |p_x^b - 1000| < \eta_{ba} \\ \sigma_{a_x}^2 \ll \sigma_{r_x}^2, & \text{otherwise} \end{cases} \quad (23)$$

Testing

In this section, the testing procedure, sketched in Figure 3, is described in detail.

Multibody model of the railway vehicle

The development and calibration of the odometric algorithm, described in the section on sensor fusion between odometers and INSs, involves the availability of coherent kinematical inputs (wheel angular speed, acceleration and angular orientation) and the simulation of a wide range of working conditions, whose realization by means of experimental test runs is difficult and expensive.

On the other hand, for this type of application, the use of commercial multibody software is quite difficult, since the simulation of degraded adhesion conditions involves the co-simulation of on-board mechatronic devices, such as WSP, anti-skid, etc.

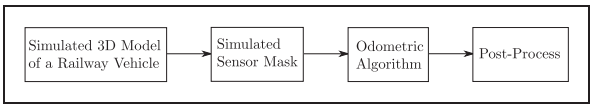

Figure 3. Testing procedure.

In order to overcome all these problems a complete 3D multibody model of a railway vehicle has been developed using Matlab-Simulink™ (see Figure 4),[18,15] which is able to reproduce different working conditions, with arbitrary tracks, including ones that may stress the behaviour of the sensors, in order to investigate their critical aspects.[15]

In particular, the 3D multibody model of a high-speed train was implemented. A single unit, composed of a coach connected to two bogies, was modelled. Using a multibody approach, the system is divided into one coach, two bogie frames, eight axle boxes and four wheelsets. The coach is held by a rear and front bogie with a two-stage suspension system (Figure 5). The railway vehicle has a $B_0 - B_0$ wheel-and-axle set (each bogie has two mechanically independent engine axles).

The railway vehicle is provided with a double suspension stage (first and second stages in both vertical and lateral directions) between the coach, the bogies and the axles, damping devices (vertical, lateral, anti-yaw dampers) with non-linear characteristics, anti-roll bar and bump-stop plugs (to reduce the carbody roll motion, and other coach motions, respecting the vehicle loading gauge).

Force elements (e.g. the two suspension stages and the bump stops) have been modelled by means of springs and dampers, with opportunely defined non-linear characteristics reproducing the real component

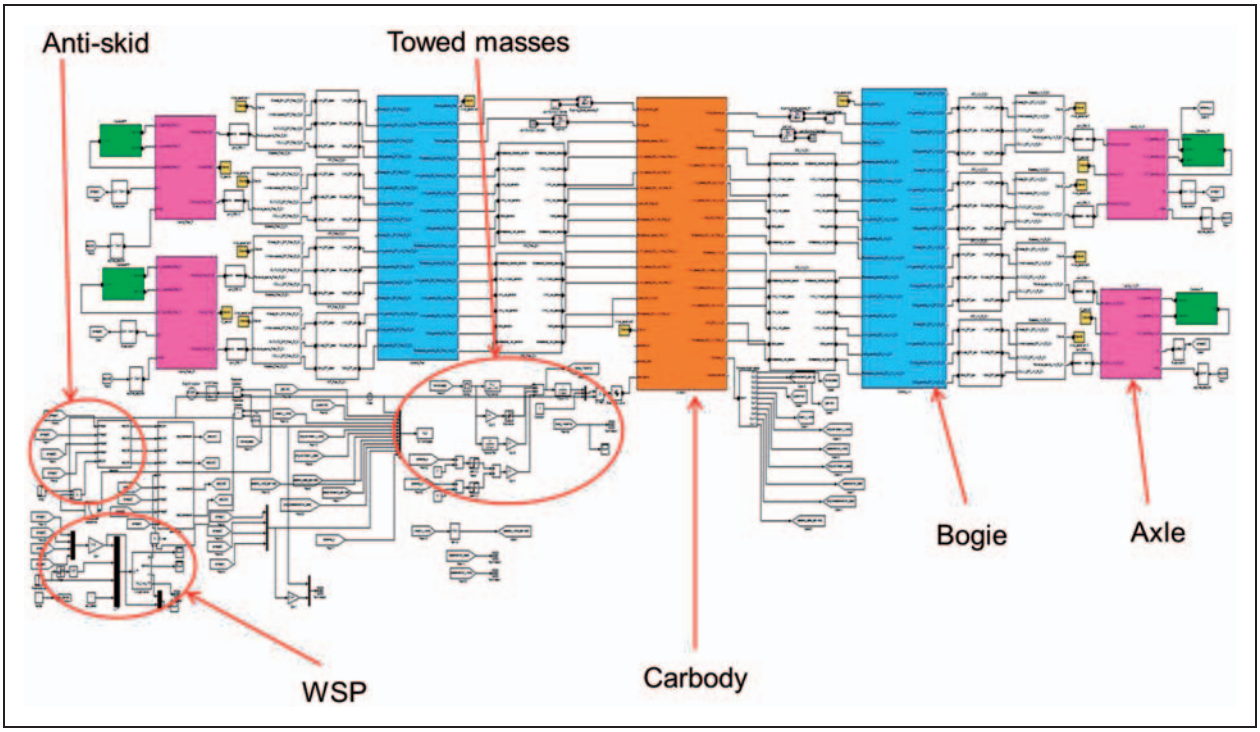

Figure 4. Simulink schema of the multibody model.

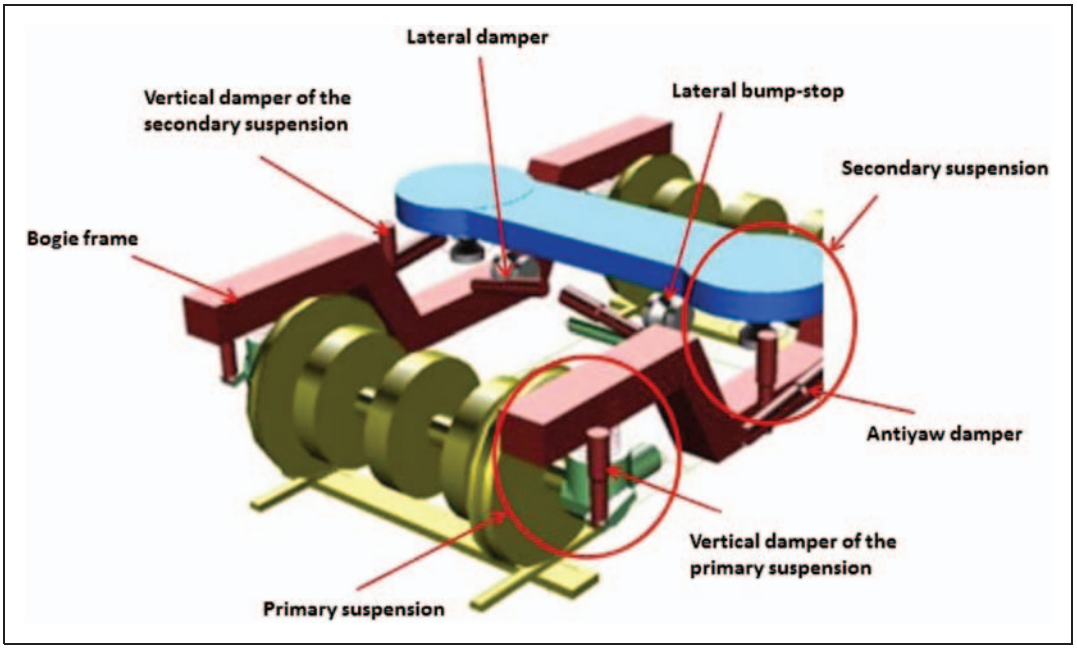

Figure 5. Two-stage suspension bogie model.

Table 1. Main characteristics of the vehicle model.

Parameter	Units	Value
Total mass	kg	$\approx 56,000$
Wheel-and-axle set	–	$B_0 - B_0$
Bogie wheelbase	m	2.42
Bogie distance	m	16.9
Wheel diameter	m	0.92
Primary suspended masses own frequency	Hz	≈ 4.5
Secondary suspended masses (carbody) own frequency	Hz	≈ 0.8

behaviour (the data reproduce, in a quite realistic way, the typical properties of a high-speed train).

In Table 1, the main properties of the rail vehicle are shown. In Table 2, the elastic characteristics of the connection elements are displayed.

Vertical and lateral damping devices ensure a relatively high damping of the modes of vibration of the system: these elements are modelled with non-linear characteristics to reproduce the real behaviour. The wheel profile used for the simulations is the standard International Organization for Standardization (ISO) Office de Recherches et d'Essais de l'Union Internationale des Chemins de fer (ORE) S1002, while the rail profile is a International Union of Railways (UIC)60 with a 1/20 cant.[19]

For the motion resistance and the possible presence of the towed vehicles, the authors considered resistant contributions, such as the cushion friction and the aerodynamic resistance, applying a longitudinal force to the centre of mass of the coach; the overall resistance is modelled according to a second-order polynomial function of the longitudinal speed whose coefficients are estimated in accordance with the data available in the literature.[20,21]

The simulated tests have the following characteristics:

- long time running: in order to have high INS integration errors;
- degraded adhesion: in order to stress tachometer measures;
- line gradient: it significantly affects the accelerometer error, see equation (15);
- curves and cant angles: a good estimation of the line gradient in the orientation Kalman filter is influenced by a good estimation of yaw and roll angles;
- patterns of irregularities of the rail line (rail gauge irregularities, cant, etc.).

In order to guarantee the robustness and the safety of the proposed solution, the odometric algorithm has to be tested with a huge number of long paths, so that a strong computational effort is involved. In order to avoid it, some basic modules with a great variability of features have been simulated. Longer tracks can be then created settling these basic modules the one with the other; in this way, the computational effort is distributed on a limited set of short simulations.

Simulated sensor masks

The accelerations and angular rates reproduced by the Matlab-Simulink^{TM} model have been processed by a mask that simulates the sensor errors described in the section on sensors for odometry. The quantification of the errors was carried out by the experimentation of a custom IMU designed by ECM S.p.A. based on low-cost MEMS inertial sensors (Figure 6).

Table 2. Elastic characteristics of the two-stage suspension.

Element	Translational Stiffness x (N/m)	Translational Stiffness y (N/m)	Translational Stiffness z (N/m)	Rotational Stiffness x (Nm/rad)	Rotational Stiffness y (Nm/rad)	Rotational Stiffness z (Nm/rad)
Primary suspension	844,000	844,000	790,000	10,700	10,700	0
Secondary suspension	124,000	124,000	340,000	0	0	0
Axlebox bushing	4,0000,000	6,500,000	4,0000,000	45,000	9700	45,000
Anti-roll bar	0	0	0	2,506,400	0	0

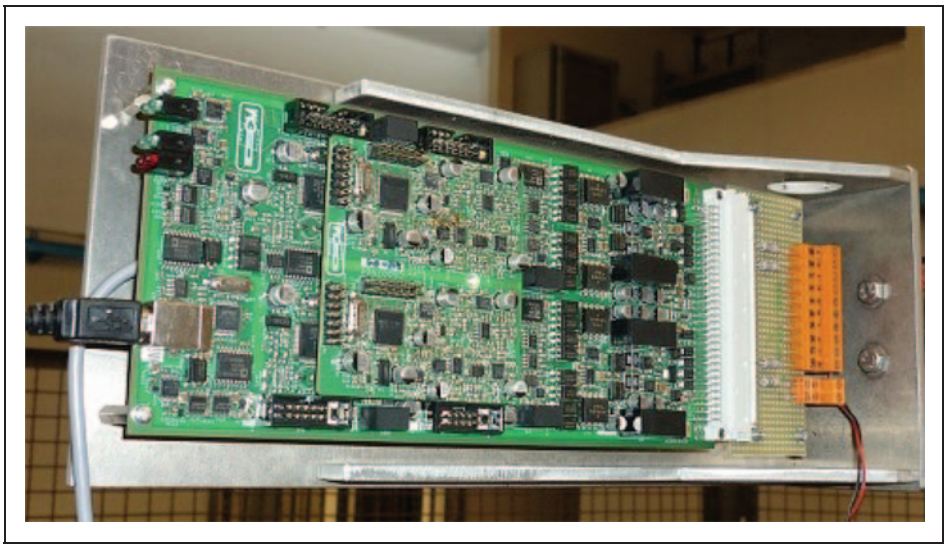

Figure 6. Custom IMU board.

Table 3. Errors of sensors.

Parameter	Units	Value
η_a	m/s^2	2.2×10^{-3}
η_g	rad/s	7.8×10^{-4}
b_a	m/s^2	4.1×10^{-3}
b_g	rad/s	2.5×10^{-5}
η_m	rad	2.2×10^{-4}

The following assumptions have been checked by the IMU testing:

- random noise has been simulated, both for the accelerometer and for the gyroscope, as a Gaussian white noise with zero mean and standard deviation, η_a and η_g, as in Table 3;
- deterministic biases have not been simulated, since they are supposed to be removed during the calibration phase;
- random biases, b_a and b_g, have been simulated with the values given in Table 3;
- scale-factor errors have not been simulated, since they do not influence the results: in fact, since the range of interest for the measurements is very limited, its influence in the output is not relevant, and no error of this kind appeared during the tests;
- a thermal analysis, performed in the climate chamber of Figure 7, has shown the presence of a relevant error related to the temperature in the range [-20° to 55°]. In Figure 8, the 'error versus temperature' graph is reported for an axis of both the accelerometer and the gyroscope;
- no linear drifts have been detected during the experimentation;
- a 2° assembly error has been simulated for each Euler angle, which was obtained from the experience of the manufacturers. This error could be removed for roll and pitch angles through an initial gravity calibration. The inaccuracy that persists after this procedure has been simulated with a zero-mean Gaussian noise with standard deviation η_m, as in Table 3.

The values η_a, b_a and η_g, b_g are obtained, respectively, from the data sheet of the accelerometer and the gyroscope used in the custom IMU board.

Post-processing and evaluation of the performances of the algorithm

Since the inertial sensors are affected by stochastic noise, the efficiency of the algorithm cannot be evaluated analytically. Monte Carlo runs are made to

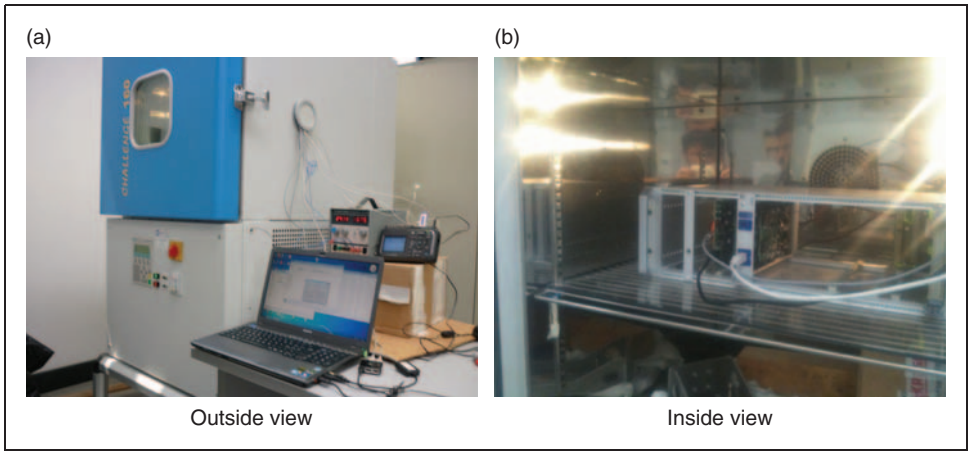

Figure 7. Thermal analysis performed on the climate chamber at ECM.

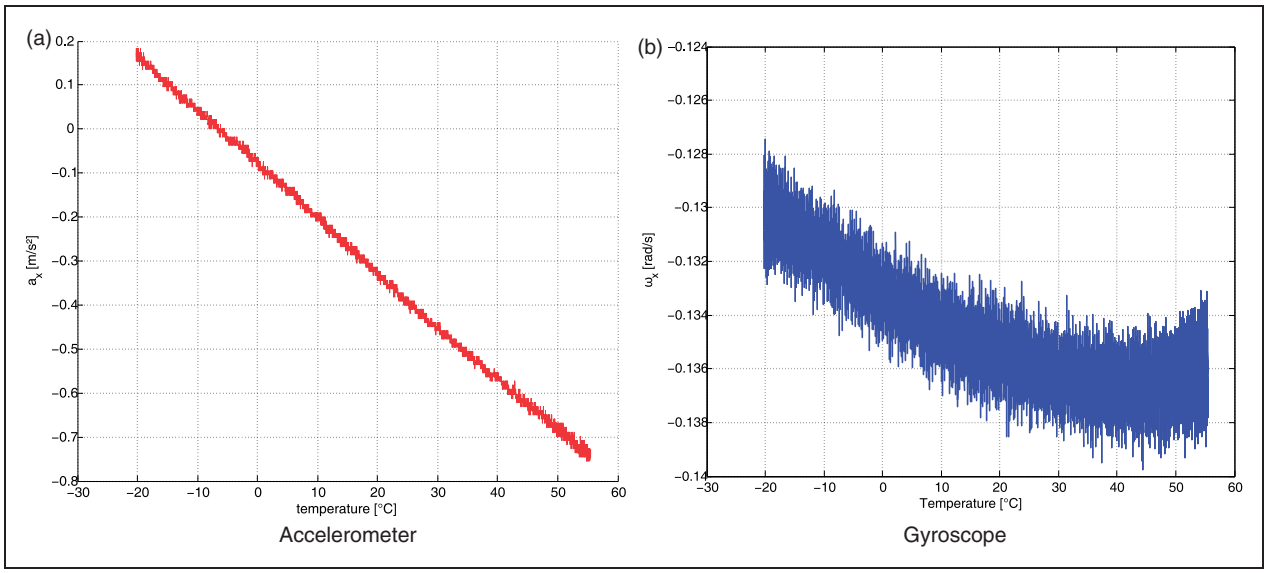

Figure 8. Error versus temperature graph.

obtain an estimation of the expected value of the performance from a sample average of independent realizations.[22] A large number of runs increases the power of the hypothesis testing. The performance estimation relative to N independent runs is the mean of the N cost values

$$\bar{C} = \frac{1}{N}\sum_{i=1}^{N} C_i \tag{24}$$

where the ith cost value C_i is the error between the true and the estimated travelled distance ($\tilde{p}_x^b = p_x^b - \hat{p}_x^b$) or speed ($\tilde{v}_x^b = v_x^b - \hat{v}_x^b$).

The mean error between true and estimated speed (or travelled distance) can be compared with the same cost obtained with the SCMT algorithm, described in the subsection on wheel angular speed sensors (tachometers).

The performance parameter used to evaluate the advantages of the localization algorithm in terms of reliability is the percentage of time the signal error does not meet the ETCS requirements (blue line in Figure 9),[1,2,3,4] i.e. the maximum acceptable error of speed (position) as a function of the current train speed (travelled distance).

As will be detailed in the following section, the proposed localization algorithm allows speed and travelled distance errors much lower than the values imposed by the ETCS requirements to be obtained, and the results are compared with error limits stricter than the ETCS values, equal, respectively, to one half, one quarter and one eighth of the ETCS limit. These reduced performance thresholds are shown in Figure 9.

Results

The testing procedure has been applied to ten worst-case-design paths, whose features are summarized in Table 4. Every path consists of three phases of

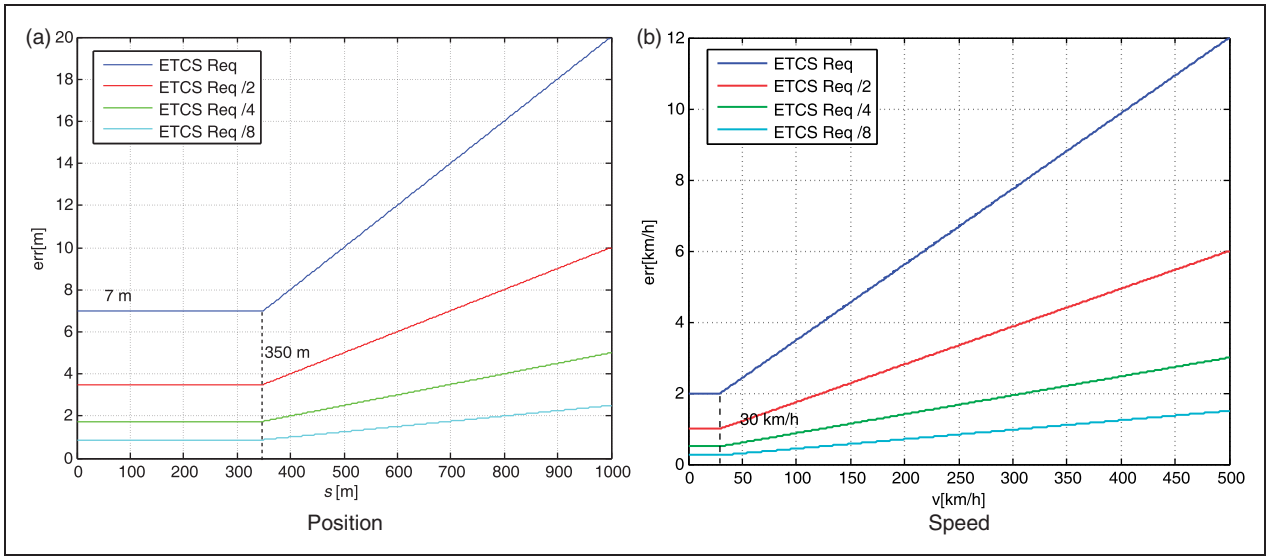

Figure 9. ETCS requirements: reference (blue line) and reduced values.

Table 4. Testing paths: characteristics.

ID	Degree of criticality	Characteristics
1	High	Articulated altimetry, with uphills and downhills up to 30‰, without any curves
2	High	Curved track with a radius of curvature of 1800 m, but level (there are no uphills or downhills)
3	High	Combination of curves (radius of curvature of 1800 m) and slopes (uphills and downhills up to 30‰)
4	High	Curves (radius of curvature of 1800 m) and uphills (downhills) with mixed slopes (10, 20, 30‰)
5	High	Very similar to the previous ones, but the curves are faced at such a speed and with a radius of curvature that the lateral acceleration is zero (testing of the criticality of the roll reset)
6	Very high	Very long (nearly 30 km) with slopes in the coasting phase
7	Very high	The first uphill, with slope of 30‰, is faced at a speed of about 15 km/h (testing if the gyroscope can read the angular rates over the *y* axis)
8	Very high	The first uphill, with a slope of 10‰, is faced at a speed of 35 km/h (same objective as the previous)
9	Very high	Very similar to the 7th, but the facing speed is about 8 km/h
10	Very high	The first curve (radius of curvature of 10000 m) is faced at speeds below 40 km/h (testing if the gyroscope can read the angular rates over the *z* axis)

traction and braking, affected by degraded adhesion and interspersed by a phase of coasting. For the adhesion, the railway paths have some sections characterized by good adhesion conditions, with a static adhesion coefficient equal to 0.3 (no slidings between the wheel and the rail), and some sections under degraded adhesion conditions, with a static adhesion coefficient equal to 0.1 (slidings between the wheel and the rail occur).

A degree of criticality (high or very high) is assigned to each testing path, in relation to the features that highlight the weaknesses of the sensors. The first five are characterized by a high degree of criticality, since the changes of slopes and the curves are faced at such a speed that the angular rates are greater than the noise of the gyroscope. The last five paths are characterized by a very high degree of criticality due to the high level of stress imposed on the sensors, in particular, it is checked if the gyroscopes are able to detect the angular rate in very extreme conditions due to very low train speeds and very limited slope transients of the line gradient.

For instance, the simulated data from the inertial sensors, related to path # 3, are reported in Figure 10.

Tables 5–7 show a quantitative description of each path, in terms of length, percentage of degraded adhesion, range of speeds, distribution of the slopes of the track and rate of curvature of the path.

To be short, the following graphs (the 'true speed of the train' always refers to the longitudinal speed of

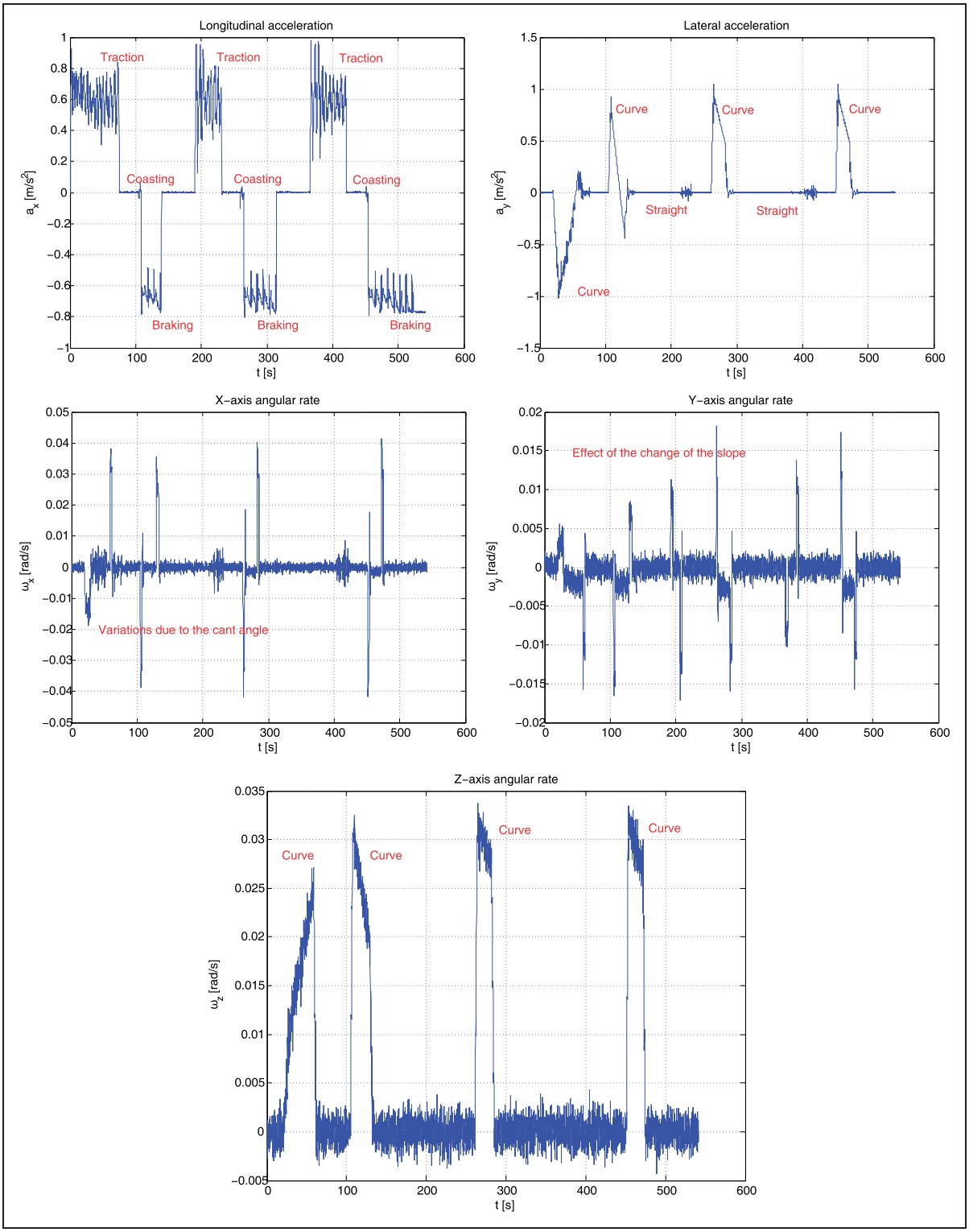

Figure 10. Simulated data from the inertial sensors, related to path # 3 (longitudinal and lateral accelerations and triaxial angular rates).

the railway vehicle during the simulations) are reported only for path # 1.

The comparison between the true speed of the train and the speed estimated by SCMT and INS/ODO algorithms (Figure 11), with a zoom on the traction phase and on the braking phase (Figure 12).

In Figure 12, the accuracy enhancement provided by the innovative algorithm, compared to the SCMT solution, is manifest: although the braking conditions imposed in the simulation are critical, in terms of adhesion, the wheel peripheral speed is very far from the 'true' one, and the contribution of the INS algorithm allows a good estimation with a very low drift.

Table 5. Testing paths: length and percentage of degraded adhesion and distribution of speed ($v_1 = 50$ km/h, $v_2 = 150$ km/h).

ID	Length (km)	% of degree adhesion	% of speed $v < v_1$	% of speed $v_1 < v < v_2$	% of speed $v > v_2$
1	20.91	40.14	7.28	51.56	41.15
2	20.71	41.84	7.15	50.48	42.36
3	20.63	49.51	7.24	47.92	44.84
4	26.59	40.25	6.61	49.16	44.23
5	31.40	33.07	4.92	52.48	42.60
6	36.76	43.59	4.22	51.87	43.91
7	21.31	39.26	8.85	50.40	40.76
8	21.03	39.70	8.22	49.88	41.89
9	21.31	39.27	9.28	50.21	40.52
10	21.16	42.63	7.99	48.60	43.41

Table 6. Testing paths: distribution of curved track ($\dot{\phi}_1 = 1 \times 10^{-4}$ rad/s, $\dot{\phi}_2 = 0.005$ rad/s).

ID	% of yaw rate $\dot{\phi} < \dot{\phi}_1$	% of yaw rate $\dot{\phi}_1 < \dot{\phi} < \dot{\phi}_2$	% of yaw rate $\dot{\phi} > \dot{\phi}_2$
1	100	0	0
2	71.18	5.36	23.46
3	71.86	5.21	22.94
4	73.48	4.39	22.13
5	57.12	6.48	36.40
6	72.13	5.14	22.74
7	100	0	0
8	100	0	0
9	100	0	0
10	71.52	13.28	15.20

Table 7. Testing paths: distribution of sloped track.

ID	% of slopes $\theta < 5‰$	% of slopes $5 < \theta < 15‰$	% of slopes $\theta > 15‰$
1	86.96	1.37	11.67
2	100	0	0
3	73.10	2.46	24.45
4	84.22	3.21	12.58
5	83.85	4.66	11.49
6	62.91	6.95	30.15
7	83.75	2.01	14.23
8	85.82	8.15	6.03
9	82.92	2.04	15.04
10	81.07	1.74	17.19

However, the contribution of the tachometer is fundamental when the system detects a good adhesion condition.

- The comparison of the travelled distance error with the ETCS requirements, Figure 13a.

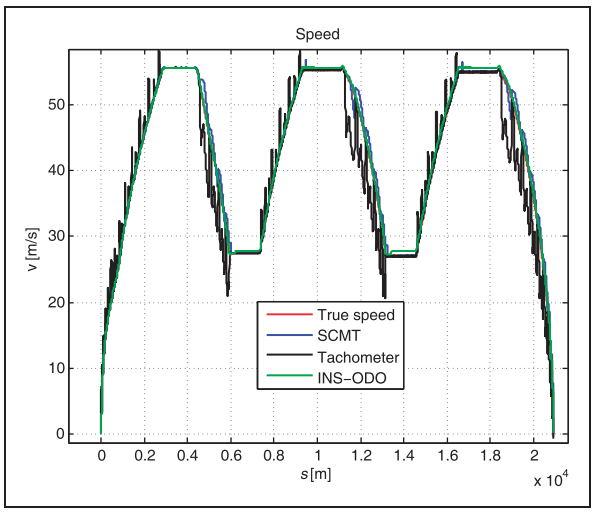

Figure 11. Comparison between true and estimated speeds.

- The comparison of the speed error with the ETCS requirements, Figure 13b.

In order to show the different performances of the algorithm, the speed errors of the 10 paths are shown in Figures 14–16.

The results show that the localization algorithm estimates are good, since the speed and the position errors are always much smaller than the speed and position requirement thresholds.

It is worth noting that the ETCS requirement thresholds should be a function of the longitudinal speed (i.e. each path has its own ETCS requirement), but, in order to have clearer graphs, the ETCS threshold used is the stricter one (to be cautious).

Figure 16 shows particulars of the critical starting phase: in fact, since the train speed is low, the angular rate measured over the y axis, although the line slope is changing, may be so small as to be incorporated into the noise.

From the picture, it is obvious that paths #7, #8 and #9, which are characterized by a slow initial

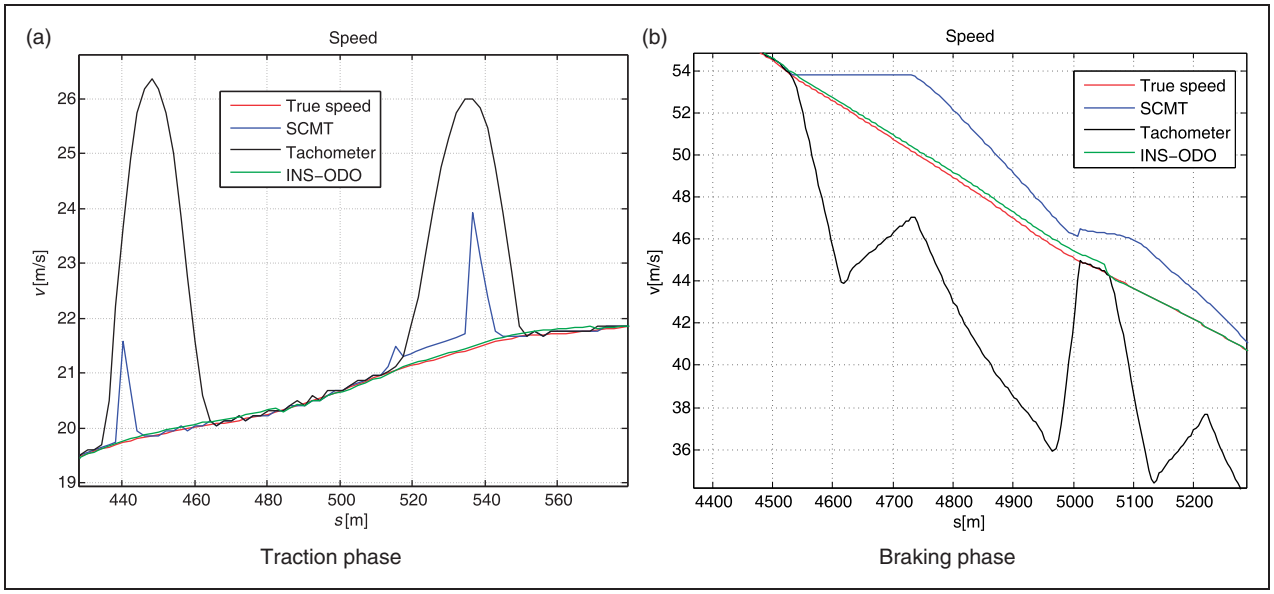

Figure 12. Comparison between true and estimated speeds – particulars.

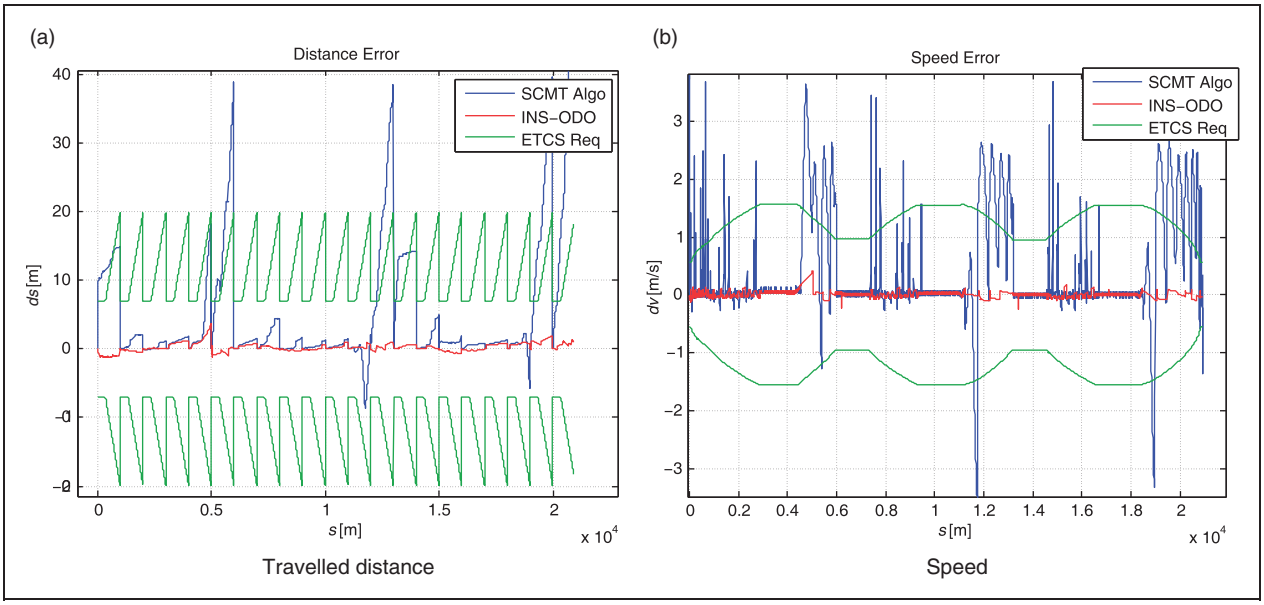

Figure 13. Errors with respect to ETCS requirements.

acceleration ramp, have worse performances in terms of accuracy, even though the error meets the ETCS requirements.

Finally, the histograms in Figure 17 summarize the performance parameters explained in the subsection on post-processing and evaluation of the performances of the algorithm, where the mean errors of speed and travelled distance are obtained after 100 Monte Carlo runs.

The results are subdivided into four sets: one with performances of speed estimation for paths with high degrees of criticality (Figure 17a), one with performances of speed estimation for paths with very high degrees of criticality (Figure 17b), one with performances of travelled distance estimation for paths with high degrees of criticality (Figure 17c) and the last with performances of travelled distance estimation for paths with very high degrees of criticality (Figure 17d).

Each figure shows, on the first planar axis, the requirement used (ETCS or its subdivisions), on the second planar axis, the ID of the path and, on the vertical axis, the value of the calculated performance parameter.

Since the results for the SCMT algorithm (blue histograms) are significant just considering the

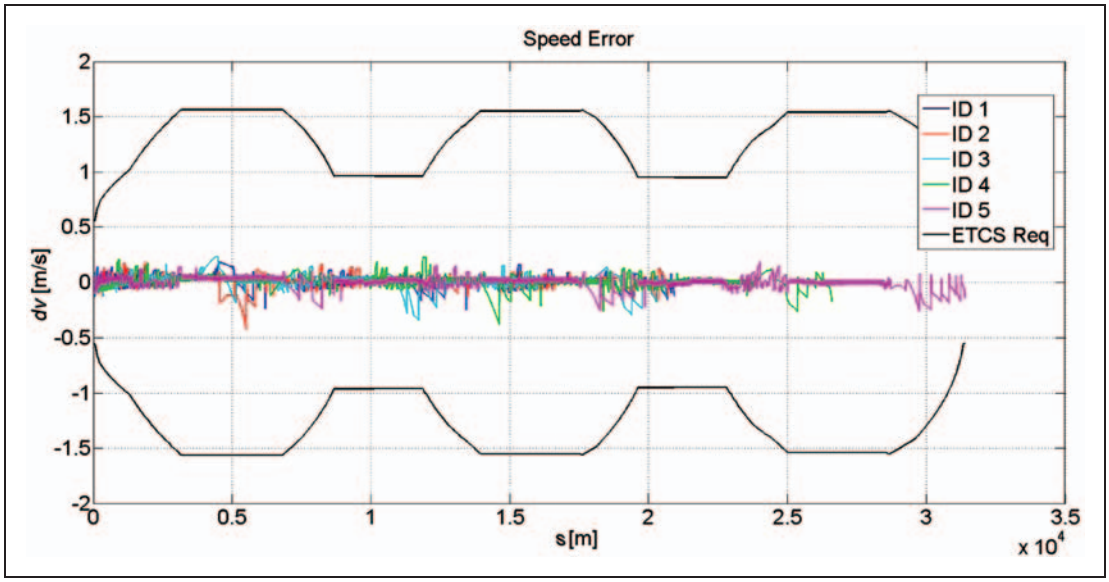

Figure 14. Paths 1–5: comparison between the speed errors and the ETCS requirements.

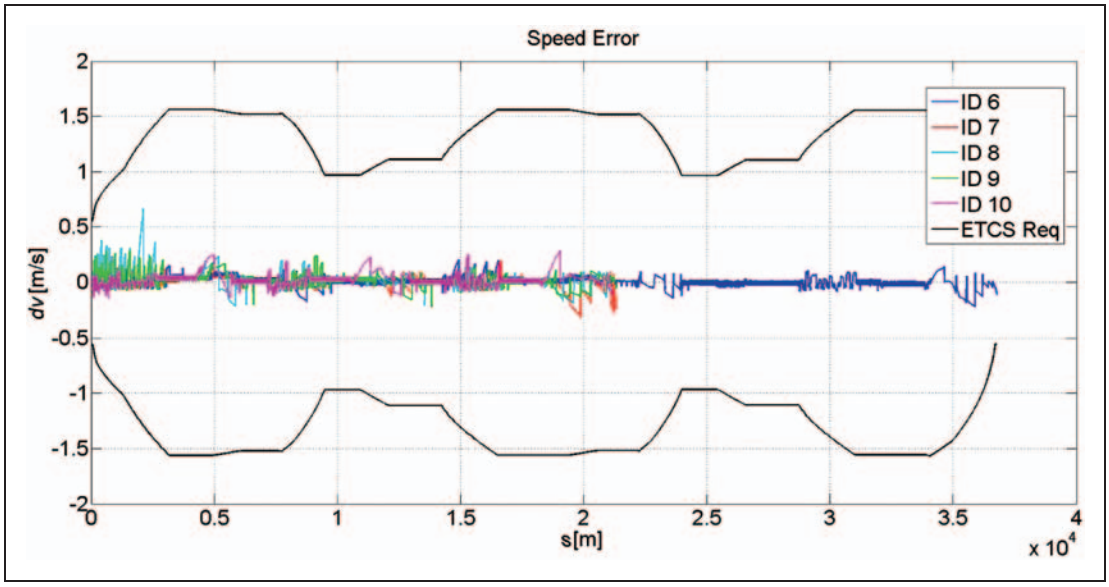

Figure 15. Paths 6–10: comparison between the speed errors and the ETCS requirements.

ETCS requirements, the comparison with its subdivisions has been performed only for the INS/ODO algorithm (green histograms).

The histograms point out some relevant results:

- although the tuning of Q and R matrices is a tricky activity (EKFs are not reliable with non-stationary signals), a suboptimal set of parameters provide good results for a wide range of heterogeneous tests;
- the innovative algorithm has a much better performance than the SCMT algorithms;
- the ETCS requirements should be kept to one eighth of its value, in order to be able to see a significant error of estimate;
- two paths (# 7 and # 8) show worse behaviour, since their performance parameter with respect to the 'official' ETCS requirements is not zero (i.e. the limit thresholds are overcome).

Conclusions

This paper describes an innovative localization algorithm that fuses the information from an odometer and an IMU, owing to the Kalman filter theory.

The main features of the localization algorithm have been summarized and the sensor output signals have been simulated through a 3D multibody model of a railway vehicle. A huge number of simulated paths with a wide range of working conditions and

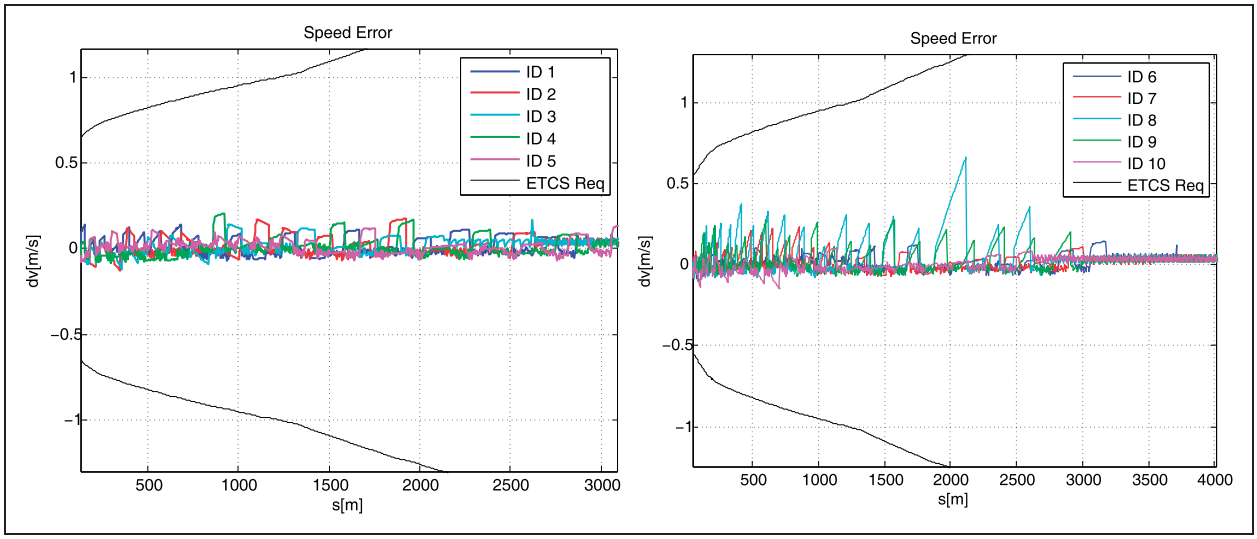

Figure 16. Paths 1–10: speed errors in the starting phase.

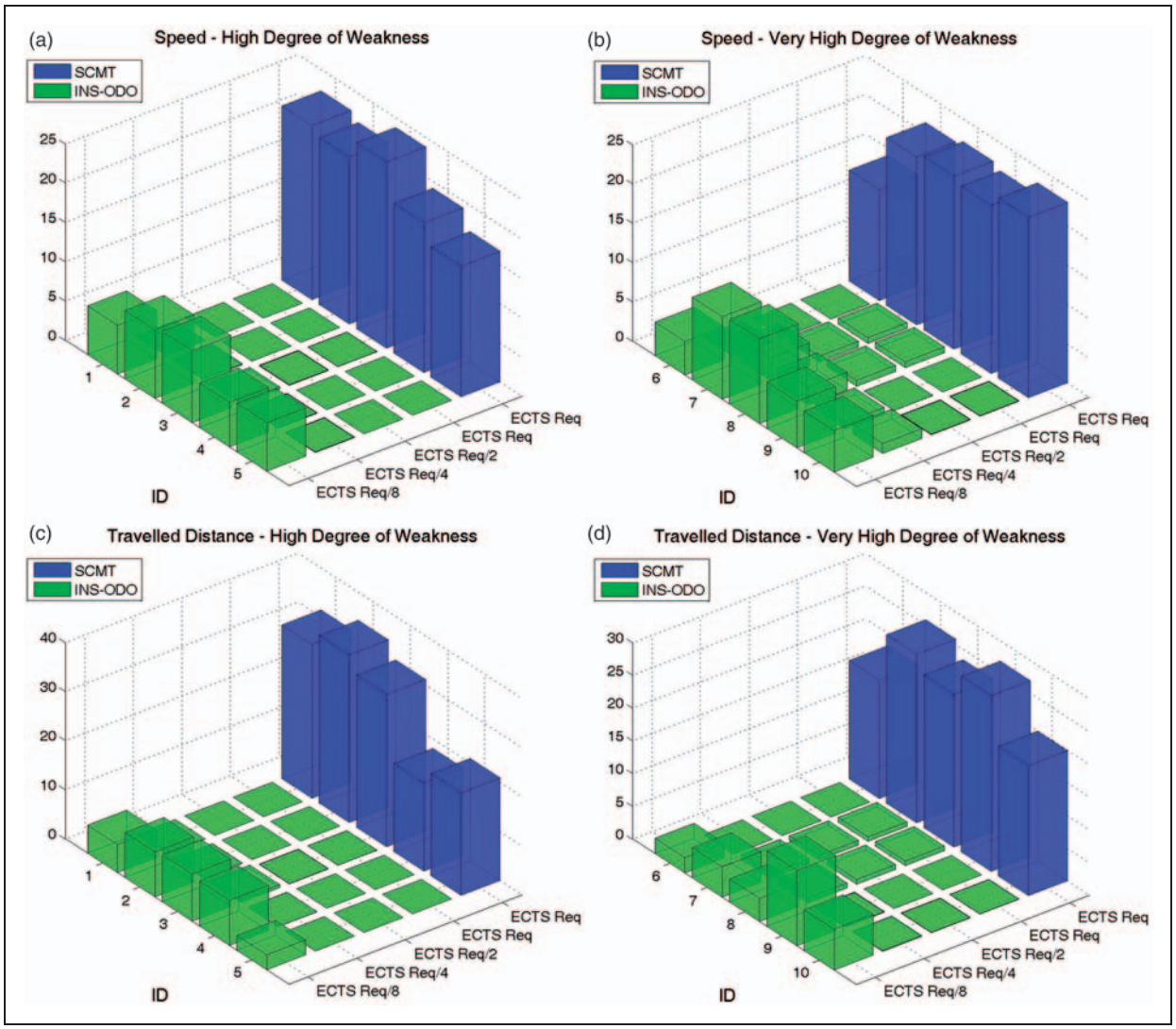

Figure 17. Percentage of time errors that do not meet ETCS requirements.

track configurations have been used to test the algorithm.

The preliminary results show a significant improvement of the position and the speed estimation, compared to the classical SCMT algorithm, using the percentage of time the error signal does not meet the ETCS requirements as performance parameter.

This paper shows the achievement of many relevant objectives, and the drawbacks of exploiting the accelerometer to detect degraded adhesion conditions have been overcome, owing to the use of a complete inertial platform that can provide a reliable estimation of the orientation of the vehicle, and of the track line. An efficient accelerometric criterion is the base for a reliable speed estimation also under degraded adhesion conditions.

Another relevant achievement is the possibility to provide only one tachometer for the odometry application; classical applications need two of them, as the minimum setting of sensors for the estimation of the sliding state (adhesion level) of the wheels. The omission of one tachometer has a relevant and positive impact on the system, since these sensors have many mechanical and maintenance problems.

Further activities will be carried out to test the algorithm performances through a wide set of experimental train runs, using a hardware-in-the-loop test rig composed of an industrial robot used as a dynamic simulator to test the custom IMU board designed by ECM S.p.A. On-track tests are scheduled for next summer.

Funding

This work was supported by ECM S.p.A. within the project COINS (Cooperative Odometry-Inertial Navigations System), funded by Regione Toscana under the program 'BANDO UNICO R&S anno 2008 - linea A'.

References

1. EEIG ERTMS Users Group. Specific transmission module FFFIS, Reference EEIG Subset-035, Issue 2.0.0, 30 March 2000.
2. EEIG ERTMS Users Group. Performance requirements for STMs, Reference EEIG Subset-059, Issue 0.0.6, 28 March 2000.
3. EEIG ERTMS Users Group. Performance requirements for STMs, Reference EEIG Subset-041, Issue 2.0.0, 30 March 2000.
4. EEIG ERTMS Users Group. Odometer FFFIS, Reference EEIG 97E2675B, Document Version 5-, 31 July 1998.
5. Malvezzi M, Bartolini F, Rinchi M, et al. Analysis of braking performance for the definition of emergency braking intervention in ATP systems. In: B Ning (ed.) *Advanced train control systems*. WIT Press, 2010.
6. UIC B126.15, C Group. Braking questions safety margins for continuous speed control systems on existing lines and migration strategy for ETCS/ERTMS. DT 407, 2005.
7. UIC B126.15, C Group. Braking questions methodology for the safety margin ETCS/ERTMS. DT 414, 2006.
8. Malvezzi M, Allotta B and Rinchi M. Odometric estimation for automatic train protection and control systems. *Veh Sys Dyn* 2010; 49(5): 723–739.
9. Ernest P, Mazl R and Preucil L. Train locator using inertial sensors and odometer. *IEEE intelligent vehicles symposium*. University of Parma, 2004, pp.860–865.
10. Heidari A, Sandidzadeh MA and Farshad S. A novel method for estimation of train speed and location using traction motor voltage and current. *Proc IMechE, Part F: J Rail Rapid Transit* 2012; 226(4): 421–433.
11. Mirabadi A, Mort N and Schmid F. Application of sensor fusion to railway systems. In: *Proceedings of the 1996 IEEE/SICE/RSJ international conference on multisensor fusion and integration for intelligent systems*, Washington DC, 1996, pp. 185–192.
12. Mirabadi A, Mort N and Schmid F. Multisensor integration methods in the development of a fault-tolerant train navigation system. *J Navigation* 2003; 56(3): 385–398.
13. Allotta B, Colla V and Malvezzi M. Train position and speed estimation using wheel velocity measurements. *Proc IMechE, Part F: J Rail and Rapid Transit* 2002; 216: 207–225.
14. Colla V, Vannucci M, Allotta B, et al. Estimation of train speed via neuro-fuzzy techniques. In: *IWANN 2003*, Mahn, Menorca, Balearic Islands, Spain, 3–6 June 2003.
15. Allotta B, Pugi L, Ridolfi A, et al. Evaluation of odometry algorithm performances using a railway vehicle dynamic model. *Veh Sys Dyn* 2012; 50(5): 699–724.
16. Titterton TH and Weston J.L. Strapdown inertial navigation technology. In: N Stewart and H Griffiths (eds) *IEE radar, sonar, navigation and avionics*. Series 17, 2nd ed. Stevenage, UK: Institution of Electrical Engineers, 2004.
17. Barshan B and Durrant-Whyte HF. Inertial navigation systems for mobile robots. *IEEE Trans Robot Automat* 1995; 11(3): 328–342.
18. Meli E, Malvezzi M, Papini S, et al. A railway vehicle multibody model for real-time applications. *Veh Sys Dyn* 2008; 46(12): 1083–1105.
19. Esveld C. *Modern railway track*. 2nd ed. Delft University of Technology, MRT-Productions, 2001.
20. Iwnicki S. *Handbook of railway vehicle dynamics*. Taylor & Francis, 2006.
21. Vicuna G. *Organizzazione e Tecnica Ferroviaria*. Rome: CIFI, 1989.
22. Bar-Shalom Y, Rong Li X and Kirubarajan T. *Estimation with applications to tracking and navigation*. John Wiley & Sons, 2001.